SVD TECHNIQUE APPLIED IN A 3D INVERSE IMAGING PROBLEM

Javier Cebeiro[a,c] and Marcela Morvidone[a,b]

[a]*Centro de Matemática Aplicada, Universidad Nacional de San Martín, Av. de Mayo y Francia, B1650HMP, Gral. San Martín, Buenos Aires, Argentina*

[b]*Grupo de Procesamiento de Señales, Dto. de Ingeniería Eléctrica, Facultad Regional Buenos Aires, Universidad Tecnológica Nacional. Mozart 2300 (C1407IVT), Ciudad de Buenos Aires, Argentina.*

[c]*CONICET*

Keywords: Conical Radon Transform, Compton scattering tomography, 3D imaging reconstruction.

Abstract. We study the validity of the numerical implementation of the direct Conical Radon Transform, the so called $T\mathbb{C}$. This operator is at the core of imaging based on Compton scattered radiation emitted by a medical object which has received an injection of radiotracer. The $T\mathbb{C}$ is basically an integral transformation over conical surfaces of fixed axis, and it models the data acquisition step in an ideal frame. The inversion of the $T\mathbb{C}$ by singular value decomposition SVD is shown to be satisfactory on a 3D Shepp-Logan brain phantom, confirming that the numerical implementation of the direct model is adequate. It also provides useful information related to the discretization of the direct problem. Finally, we analyze the applicability of the SVD technique for Compton imaging reconstruction in this 3D context.

1   INTRODUCTION

The Conical Radon Transform (CRT) family provides a mathematical model of a new principle for camera gamma imaging that takes advantage of Compton scattering to perform image reconstructions without the need for rotating the detection system around the object (Nguyen and Truong, 2002; Nguyen et al., 2004; Nguyen and Truong, 2006; Delarbre, 2005; Morvidone et al., 2010a). The invertibility of these transforms shows that the original activity function can be reconstructed from a set of projections measured at different positions with different energies but using a fixed collimated detector, resulting in a non-moving camera gamma. The 2D members in this family of transforms are: the Bi-dimensional Conical Radon Transform ($T\mathbb{V}$) and the Bi-dimensional Compounded Conical Radon Transform ($T\mathbb{V}C$). While the symbol $\mathbb{C}$ denotes an integral over the surface of a cone, $\mathbb{V}$ remarks that integration is performed over a V line, which the 2D version of the cone. Aimed at solving a 3D inversion problem, we have already been working with the CRT family. The approach is rather straightforward: after testing the invertibility of simple models the more realistic ones are explored. Full models involve more variables and incorporate the third dimension which makes its analytical inversion more complex and adds significant burden to the algebraic computation of the inverse problem. All the two-dimensional stages have already been studied and both analytical (Morvidone et al., 2010a,b, 2011) and algebraic (Cebeiro et al., 2013; Cebeiro and Morvidone, 2013b,a) inversions have been numerically implemented. The $T\mathbb{C}$ incorporates the third dimension to the problem and is more linked to the real physical model since the acquisition of projections cannot be done for a simple slice as it can be performed in the classical Radon transform. The numerical simulation of this problem involves two stages: first, generating the projections by using the direct model, and then, solving the inverse problem either by analytical or algebraic inversion. The aim of this paper is to solve the 3D direct-inverse problem using the $T\mathbb{C}$ model. We implement an algorithm for generating the projections and apply an inversion technique based in the Singular Value Decomposition of the projection matrix. Although prior results with the two-dimensional $T\mathbb{V}C$ suggest that this technique can succeed in inverting the 3D problem, several points such as stability of the solution and performance with noisy projections remain still uncertain. After generating projection matrices allowing numerical reconstruction from projections of simple and complex activity functions, we test the algorithm with projections corrupted with additive noise.

2   THE DIRECT MODEL

2.1   The Conical Radon Transform

The conical Radon transform $T\mathbb{C}$ appears in a particular imaging process introduced by T. Truong et al. in (Nguyen and Truong, 2006). The conical Radon transform of the function $f(x, y, z)$ is defined in Eq.(1).

$$T\mathbb{C}f(x_D, y_D, \omega) = g(x_D, y_D, \omega) =$$
$$\sin \omega \int_0^\infty \int_0^{2\pi} f(x_D + r \sin \omega \cos \psi, y_D + r \sin \omega \sin \psi, r \cos \omega) \, d\psi \, \frac{dr}{r} \quad (1)$$

The physical problem described by the $T\mathbb{C}$ transform concerns a 3D object in which a non uniform radioactivity source distribution exists and is represented by a nonnegative integrable activity function $f(x, y, z)$ with bounded support. Figure 1 represents the situation: a collimated linear detector is set parallel to the plane of the object, and it collects only outgoing radiation
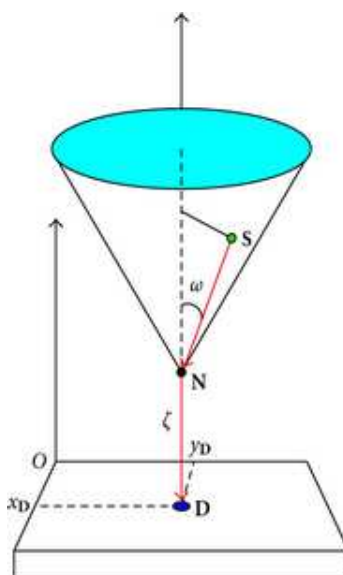
Figure 1: The setup for the 3D imaging problem.

from the object which is parallel to the direction of the collimator holes. When the detector is set to absorb gamma photons at energies below E_0, the energy of primary photons emitted by the object, the photons have undergone at least one Compton scattering at a site **N** in the bulk of the object under a scattering angle ω. The photon flux density measured at a detecting site **D** is due to the sum of scattered radiation flux densities outgoing from the set of scattering sites **N** lying along the axis of the collimator at **D**. As scattered photons have energy E, they have been deflected from an incident direction by a scattering angle ω, related to E by the Compton formula. Thus, the totality of the detected flux density for each scattering site **N** is due to the sum of all point sources lying on the cone with **N** as vertex (see coordinates of this image formation scheme in Fig. 1). For ease of notation, we shall include all physical factors resulting from Compton scattering into one term $K(\omega)$ including the square of the classical electron radius, the average electron density, and the Klein-Nishina scattering probability function.

The $T\mathbb{C}$ transform of function f in Eq. (1) represents the measured photon flux density at **D** under a scattering angle ω, assuming that the distance between the detector and the scattering media is zero, which makes sites **N** and **D** the same. It has been shown in (Nguyen et al., 2005) that this transformation is invertible, i.e., function f may be recovered from data g by means of an appropriate analytical formula. In this paper we are interested in solving the inverse problem through algebraic techniques.

2.2   The kernel of the $T\mathbb{C}$ and the Point Spread Function

Easy calculations show that the kernel of the $T\mathbb{C}$ transform, also called the Point Spread Function, PSF, has the following expression:

$$PSF(x_D, y_D, \omega | x, y, z) = \frac{\cos^2 \omega}{z^2} \delta(\cos \omega \sqrt{(x - x_D)^2 + (y - y_D)^2} - z \sin \omega). \qquad (2)$$

This concept is an analytical construction that represents the kernel of the transform and which is strongly linked to the result of applying the direct model to simulate projections of a
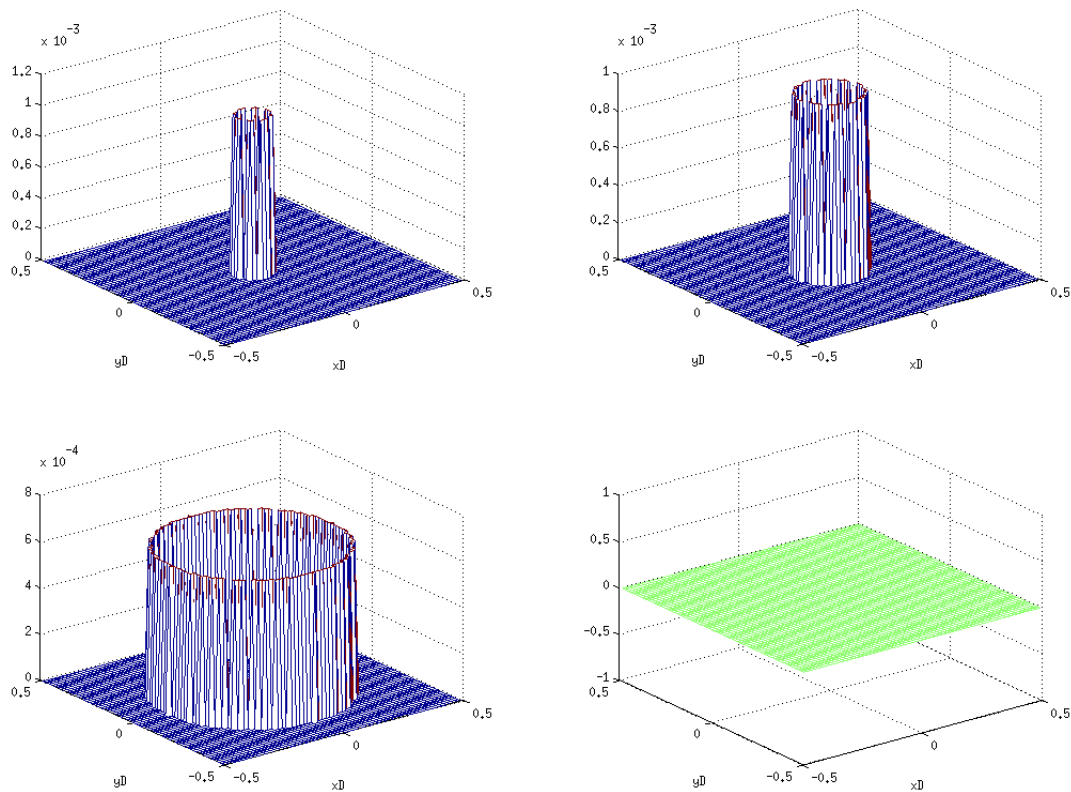
Figure 2: Central point source projections at scattering angles $w = 7°, 14°, 35°$ and $68°$

punctual source at different positions an in different scattering angles.

$$g(x_D, y_D, \omega) = \int \int \int dx \, dy \, dz \, \text{PSF}_{T\mathbb{C}}(x_D, y_D, \omega | x, y, z) f(x, y, z) \tag{3}$$

As we can see in equation (2) the non-zero values of this projections are located over the edge of a circumference centered in the point (x, y) whose equation is given in the argument of the delta function $\sqrt{(x - x_D)^2 + (y - y_D)^2} = z \tan(\omega)$. Figure 2 illustrates this idea for a central source point $(PSF(x_D, y_D, \omega | 0, 0, 0))$, notice that at scattering angle $w = 68°$ all values are zero because the source point is out of the surface spanned by the cone walls for this angle.

2.3 Algebraic formulation of the $T\mathbb{C}$

Our aim is to describe the $T\mathbb{C}$ as a linear system and then apply linear techniques for inverting the transform. This approach consists in discretizing the projection formula and applying it to a canonical basis, leading, thus, to a system of linear equations. The activity function $f(x, y, z)$ is a function of compact support in a cube of dimensions $N \times N \times N$. Such a function can be written as a linear combination of basis functions Φ_i:

$$f(x, y, z) = \sum_{i=0}^{N^3} f_i \Phi_i(x, y, z). \tag{4}$$

where Φ_i is the characteristic function of point i, defined by:

$$\Phi_i(x,y,z) = \begin{cases} 1, & \text{if } (x,y,z) = \text{ point } i \\ 0, & \text{otherwise} \end{cases} \tag{5}$$

A basis for cubic mediums (N^3 grid-points) consists of a set of N^3 different cubes Φ_i, each one containing only one point set to one and the rest set to zero. Now, the value of the projection at one point of the projection space is:

$$g_j = g(x_{D_l}, y_{D_m}, \omega_k) = [T\mathbb{C}f](x_{D_l}, y_{D_m}, \omega_k) = \sum_{i=1}^{N^3} f_i [T\mathbb{C}\Phi_i](x_{D_l}, y_{D_m}, \omega_k) = \sum_{i=1}^{N^3} A_{ji} f_i \tag{6}$$

where g_j is the value of the projection with angle ω_k at the two-dimensional detector (x_D, y_D). In a system having $D \times D$ detectors and P scattering angles, indices assume the following values: $1 \leq k \leq P$, $1 \leq l \leq D$, $1 \leq m \leq D$ and $1 \leq j \leq D^2 P$.

Then, the matrix formulation of the image formation process reads:

$$\mathbf{g} = A\mathbf{f} \tag{7}$$

Here $\mathbf{g}$ is the projection vector, each of its components is a projection value, and its size is $D^2 P \times 1$, $\mathbf{f}$ represents the object of interest, its size is equal to the number of points in the discretization $N^3 \times 1$, and finally A is the projection matrix, its size is $D^2 P \times N^3$.

Expression (7) is strongly linked to expression (1) since: $\mathbf{g} = g(x_D, y_D, \omega)$, $\mathbf{f} = f(x,y,z)$ and the product $A\mathbf{f}$ represents the action of the $T\mathbb{C}$ over $f(x,y,z)$. This algebraic formulation of the problem is in some sense the discrete relative of equation (3).

3 INVERSE PROBLEM

3.1 Inversion using Singular Value Decomposition

As stated in the previous section, the direct problem described in Sec. 2.1 can also be presented as a linear system, $\mathbf{g} = A\mathbf{f}$, where $\mathbf{g}$ is the projection measured at detectors, $\mathbf{f}$ is the original activity function and A the projection matrix. Inversion consists in finding the original function $\mathbf{f}$ from projection data $\mathbf{g}$. Since a straightforward inversion is not always possible, algebraic methods provide reconstruction using either iterative (Cebeiro et al., 2013; Herman and Mayer, 1993; Guan and Gordon, 1994; Lu and Yin, 2004; Andersen and Kak, 1984; Driol, 2008) or single step (Driol, 2008; Selivanov and Lecomte, 2001; Shim and Cho, 1981) algorithms. In scattered radiation problems, we have already tested analytical (i.e. back-projection) (Morvidone et al., 2010a,b, 2011) and iterative (i.e. Adaptive Algebraic Reconstruction Technique with a Random Permutation Scheme, RPS-AART) algorithms (Cebeiro et al., 2013; Cebeiro and Morvidone, 2013b,a).

The SVD factorization is a non iterative method which enables algebraic inversion. Let A be an $m \times n$ matrix, it can be factorized in the form:

$$A = U_{m \times m} \times S_{m \times n} \times V_{n \times n}^t \tag{8}$$

where U and V are orthogonal matrices whose columns are eigenvectors of AA^t and A^tA respectively and S is a diagonal matrix containing the singular values of A,

$$S = \text{diag}(\sigma_1, \ldots, \sigma_r, 0, \ldots, 0) \in \mathbb{R}^{m \times n},$$

where r is the rank of the matrix A. This factorization allows us to write the pseudo inverse $A^\dagger$

$$A^\dagger = V \times S^{-1} \times U^t, \tag{9}$$

and then

$$\tilde{\mathbf{f}} = A^\dagger \mathbf{g} \tag{10}$$

is the solution to the linear least-squares problem $\min \|A\mathbf{f} - \mathbf{g}\|$.

Our main aim here is to validate the implementation of the direct model, and this will be supported by a successful reconstruction from projections. In previous works we showed that inversion by SVD decomposition provides high quality reconstructions for the two-dimensional Compton imaging models (T$\mathbb{V}$ and T$\mathbb{V}$C) (Cebeiro and Morvidone, 2013b,a). This method has the advantage that the algorithm does not need to be fit by adjusting parameters such as number of iterations or permutation order, as required by iterative methods (Cebeiro et al., 2013). For a detailed description of this method as well as its imaging applications see Selivanov and Lecomte (2001); Shim and Cho (1981); Hansen (1986); Burden and Faires (2010).

3.2   Regularization by truncation

A major concern when solving an inverse problem is that a small perturbation of data $\mathbf{g}$ may lead to a large perturbation of the solution. As suggested in Hansen (1986), we use SVD truncation (TSVD) as a regularization technique, *i.e.*, the components of the solution corresponding to the smallest singular values are neglected, since these contributions to the solution are most likely to be large. More precisely, the TSVD of A is defined as the matrix

$$A_k = U \times S_k \times V^t,$$

where $S_k = \mathrm{diag}(\sigma_1, \ldots, \sigma_k, 0, \ldots, 0) \in \mathbb{R}^{m \times n}$, *i.e*, S_k equals S with the smallest $n-k$ singular values replaced by zeros, and $k \leq r$. The TSVD solution to (7) is

$$\tilde{\mathbf{f}}_k = A_k^\dagger \mathbf{g},$$

where

$$A_k^\dagger = V S_k^\dagger U^t, \quad S_k^\dagger = \mathrm{diag}(\sigma_1^{-1}, \ldots, \sigma_k^{-1}, 0, \ldots, 0) \in \mathbb{R}^{n \times m},$$

is the pseudo inverse of A_k.

4   NUMERICAL SIMULATIONS

4.1   Projections

The projections simulation $g(x_D, y_D, \omega)$ was carried out using the data acquisition model given in equation (1). The object under study is inside a cubic volume of size $N \times N \times N$. The volume is placed over a planar square detector array having $D \times D$ detectors. We considered P discretization values of the scattering angle in the open interval $(0, 90°)$, leading to an angular resolution $\Delta\omega = \frac{90°}{P-1}$. For the numerical integration a bilinear interpolation algorithm was applied to calculate the function value at points where the coordinates did not fit grid points.

In this work we present results using two different angular resolutions, $\Delta\omega = 6°$ and $\Delta\omega = 3°$ (corresponding to $P = 16$ and $P = 32$ scattering angles, respectively). For the remaining parameters, the discretization was fixed to $D = N = 16$, $\Delta r = 1$, and $\Delta\psi = 0.1$.

Figure 3 illustrates projections of the Shepp-Logan phantom, a standard object for testing medical imaging methods, in the case $D = N = 64$, $\Delta r = 1$, $\Delta\psi = 0.1$ and $\Delta\omega = 1.42°$, corresponding to $P = 64$ different scattering angles.
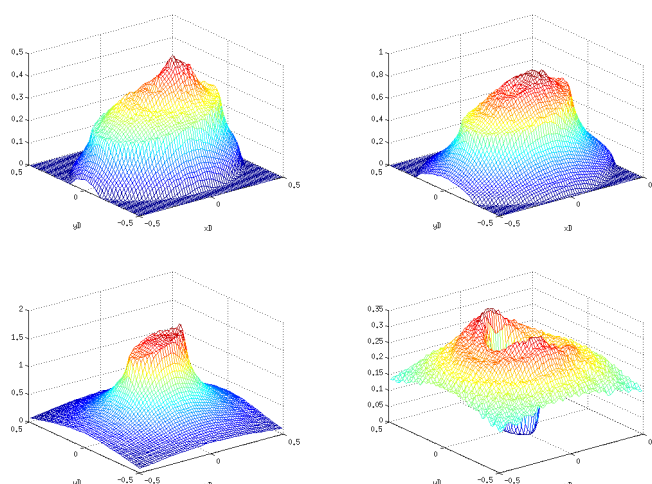
Figure 3: Shepp Logan phantom projections at scattering angles $w = 7°, 14°, 35°$ and $68°$
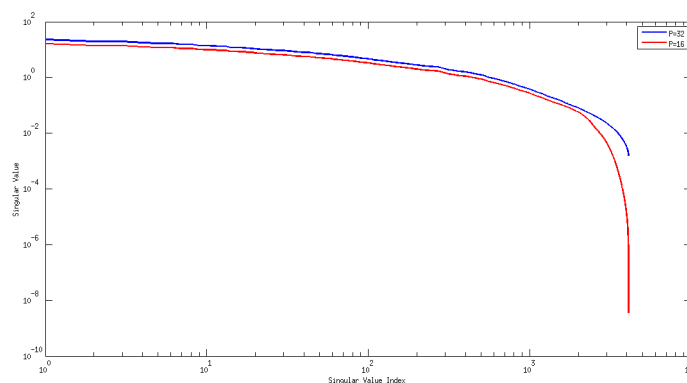

Figure 4: SVD spectra of matrix A with $P = 16$ (red) and $P = 32$ (blue) in log-log scale

4.2 Projection matrix

As stated in Sec. 2.3, the projection matrix is obtained by the action of the $T\mathbb{C}$ transform on each element of the canonical basis of $\mathbb{R}^{N^3}$. We used the discretization parameters described in Sec. 4.1 for computing the projection matrix, leading to a matrix A of size 4096×4096, when the number of angles is $P = 16$, and size 8192×4096, when $P = 32$. The matrix A is decomposed using SVD factorization. Figure 4 shows the singular values of matrix A in logarithmic scales. Note that the singular values are smaller when the number of projections diminishes, so more unstabilities are expected in the presence of noise.

4.3 Reconstructions

We perform reconstruction using the SVD pseudo-inversion as in Eq. (10). In order to assess the quality of reconstructions we used the Root Mean Squared Error (RMSE) with respect to the original phantom $\mathbf{f}$ as a figure of merit.

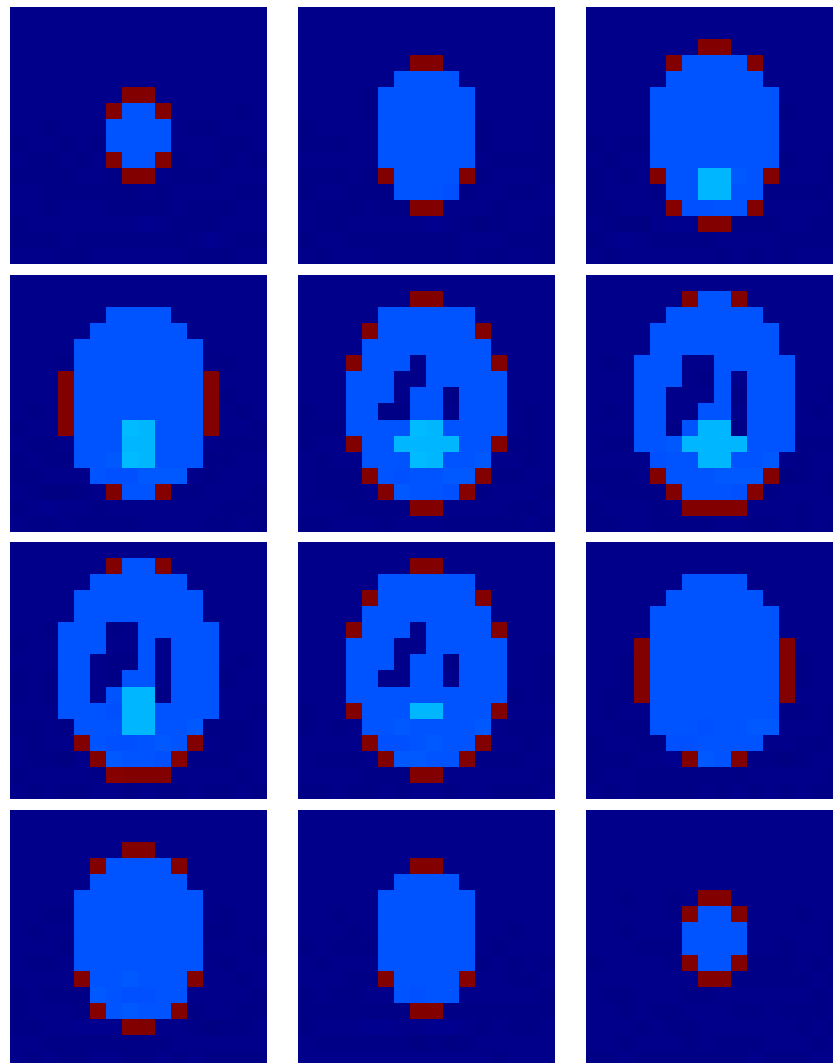$$\text{RMSE} = \|\mathbf{f} - \tilde{\mathbf{f}}\|_2$$

Figure 5: Shepp-Logan phantom reconstruction at levels z=3, 4, 5, 6, 7, 8, 9, 10, 11, 12, 13 and 14.

The RMSE was computed after image scaling in such a way that both, the reconstructed image and the original phantom, took values in the rank [0 1]. Figure 5 is an illustration of the reconstruction of the Shepp-Logan phantom, without truncation. The RMSE was 0.34%.

We perform our tests using a cylinder phantom (see Figure 6). Just as in the case of the Shepp-Logan phantom, the RMSE was small when reconstructing from noiseless data (0.2%, see Table 1).

4.4 Reconstruction from noisy projections

In a more realistic context, the data may be perturbed with noise. So, we also performed simulations considering an additive error in the data

$$g_n(x_D, y_D, \omega) = g(x_D, y_D, \omega) + n(x_D, y_D, \omega),$$

where $n(x_D, y_D, \omega)$ is a Poisson noise. Several noise levels were considered labelled by the Signal to Noise Ratio (SNR):

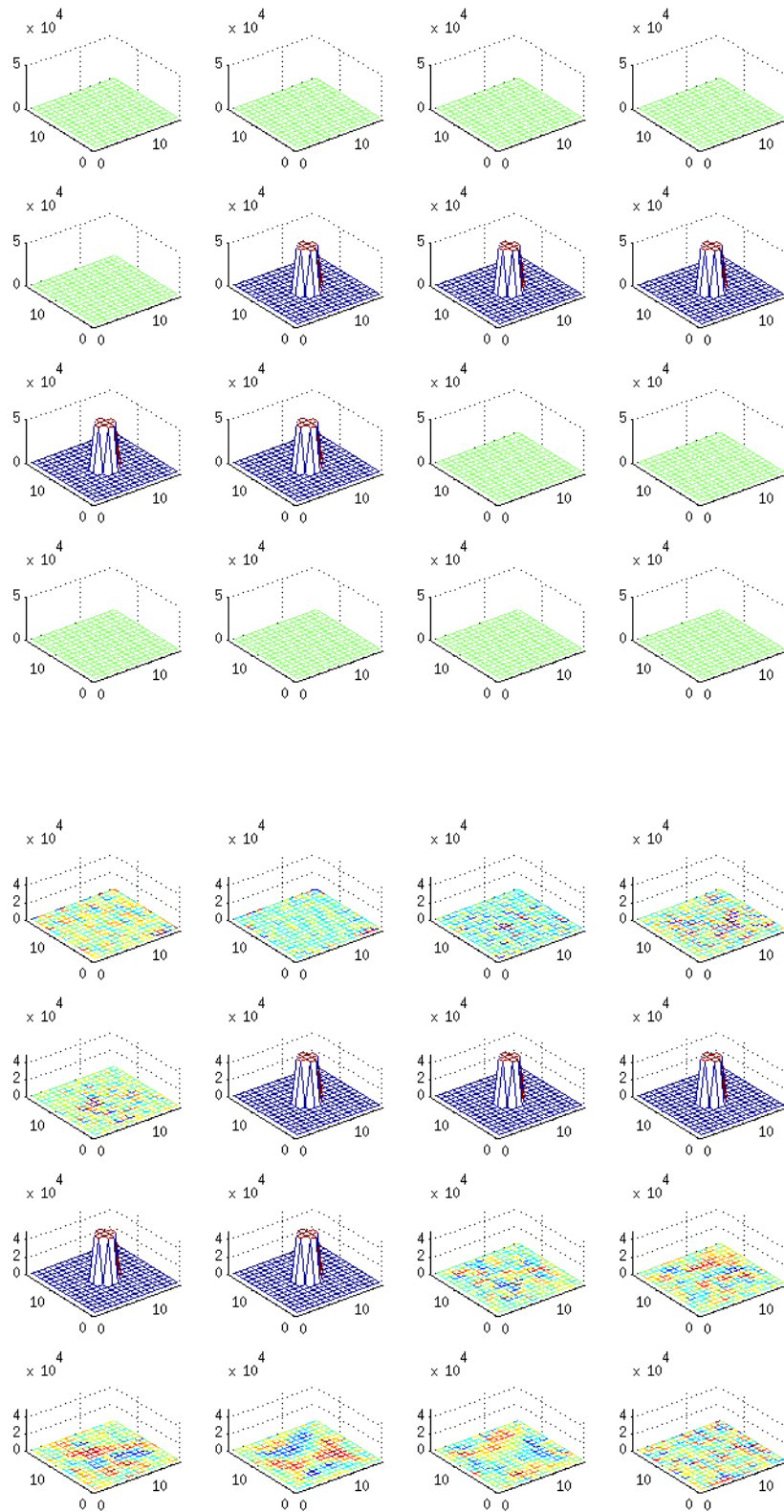$$\text{SNR} = 20 \log(\frac{\sigma_g}{\sigma_n}) \tag{11}$$

Figure 6:   Original cylinder phantom (top) and reconstructions from noiseless data (bottom).

measured in *decibels*, where σ_g and σ_n are the variances of the projections and the noise respectively. Figure 7 illustrates the projections in the absence of noise and noisy projections with a SNR= $9.2dB$. Clearly, this level of noise degrades significantly the quality of the data.

In this conditions, the inversion problem becomes unstable and a regularization method must be applied. As previously stated, we used TSVD as a regularization technique.

Table 1 shows the RMSE for different signal to noise ratios and two different numbers of angles in projections ($P = 16$ and $P = 32$). Several truncation indexes were tested. Figure 8 shows a graphic representations of these tabulated values.

k	σ_k	$P = 16$						σ_k	$P = 32$					
		Signal to Noise Ratio [dB]							Signal to Noise Ratio [dB]					
		6.6	9.2	11.7	14.9	16.8	clean		6.6	9.2	11.7	14.9	16.8	clean
4096	3.6^{-9}	49.2	46.8	50.2	55.3	46.0	**0.2**	0.0016	43.3	57.6	47.3	46.3	52.0	**0.2**
4050	3.7^{-6}	50.7	52.1	56.1	52.4	48.3	3.4	0.0024	49.7	52.7	51.4	49.7	53.3	1.4
4000	9.4^{-6}	51.4	51.6	50.6	50.7	48.3	4.0	0.0031	45.7	55.1	51.4	45.9	56.1	1.7
3500	5.1^{-4}	44.1	58.3	46.8	46.6	52.4	8.5	0.0105	50.0	44.9	49.6	47.8	52.2	7.2
3000	0.0045	56.1	38.8	51.7	48.8	50.9	10.0	0.0226	46.8	50.5	45.3	45.1	37.1	6.9
2500	0.0176	48.2	53.9	47.4	39.2	34.2	11.5	0.0428	44.8	40.2	38.8	25.6	27.2	8.5
2000	0.0572	37.0	37.0	37.1	30.2	26.6	15.3	0.0803	36.3	34.8	31.5	24.6	25.0	14.8
1500	0.1134	29.7	26.8	21.0	18.7	16.5	12.5	0.1581	25.5	23.2	21.7	15.4	14.7	12.4
1200	0.1844	29.7	19.2	15.6	**13.6**	**13.7**	11.7	0.2541	21.9	16.3	13.9	**12.7**	**12.4**	11.9
1100	0.2185	25.1	20.5	15.9	14.5	15.2	13.6	0.3015	16.6	17.8	**13.1**	13.3	12.9	12.5
1000	0.2703	26.7	18.7	**14.1**	15.0	14.5	14.0	0.3780	17.4	**16.0**	15.6	14.1	14.1	13.7
930	0.3102	**18.6**	**16.1**	17.1	16.0	16.4	15.8	0.4334	**16.2**	16.2	16.3	15.8	16.0	15.7
900	0.3268	19.3	16.8	17.2	16.4	16.4	15.9	0.4576	16.8	16.6	16.2	15.7	16.6	15.8
800	0.4111	27.1	26.2	27.9	28.0	27.7	27.4	0.5768	29.0	28.7	28.2	27.6	28.4	27.4
Mean RMSE		36.6	34.5	33.5	31.8	30.5	11.7		32.9	33.6	31.4	28.5	29.9	10.7

Table 1: RMSE (%) for reconstructions with several levels of noise and in the absence of noise

5 DISCUSSION

High quality reconstructions were obtained from complete and noiseless data (RMSE < 0.5%). When performing the inversion by TSVD the reconstruction error naturally increased, since useful data is being discarded.

Reconstructions from noisy data exhibited important deviations but the error decreased for regularized reconstructions. When too many singular values are set to zero, the error increases again, suggesting there is an optimal value for the truncation parameter. A decision criterion for the choice of this parameter like the L-curve suggested by Hansen Hansen (2000) could be interesting to study.

Generally, a lower SNR lead to worse reconstructions but this is not a systematic result, as one may expect. This may be caused by the statistical nature of the problem, and more trials should be performed to get consistent results. Besides, the error obtained with a specific truncation in the absence of noise was never reached by the corresponding regularized solution from noisy data. Thus, the error of regularized reconstructions in the noiseless case behaves as a lower bound for the TSVD reconstruction error in the noisy context (see Fig. 8, the lower green line shows the error in the noiseless case).

The duplication in the number of projections does not improve significantly the reconstructions. Nevertheless, the minimum error for fixed SNR and k is always smaller in the $P = 32$ case than in the $P = 16$ case (compare values in bold letters on Table 1). Errors for fixed SNR
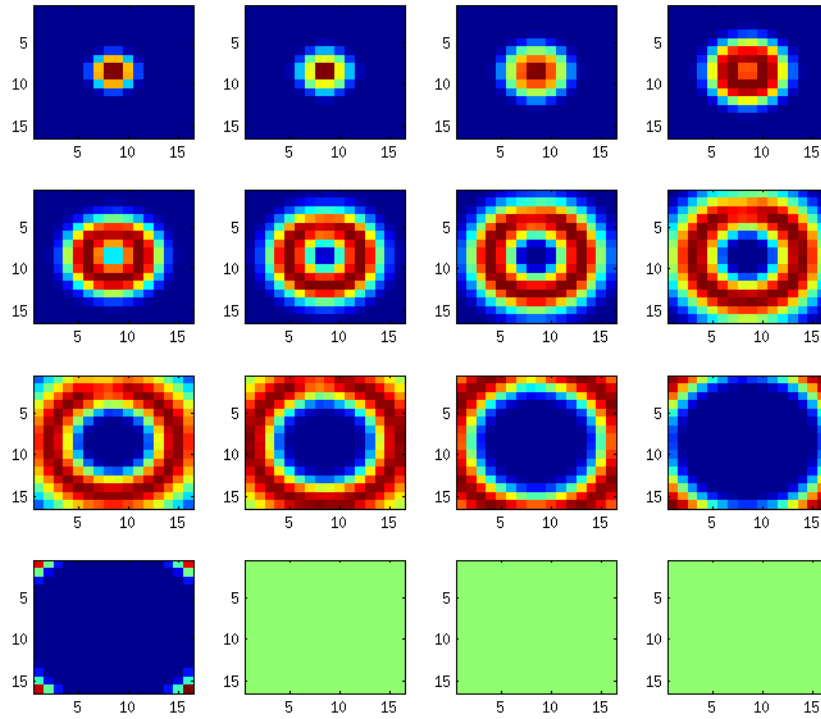
(a)
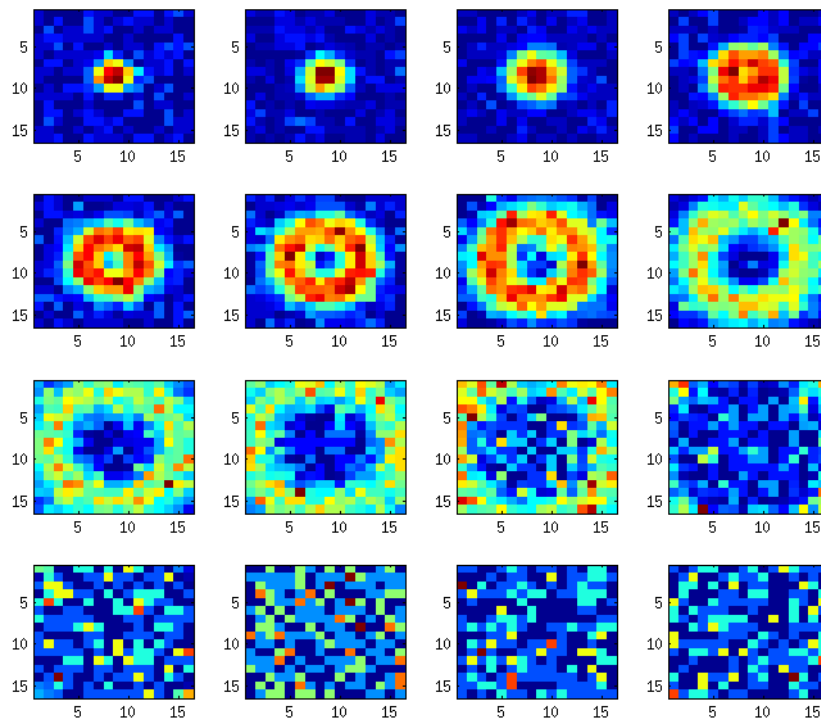
(b)

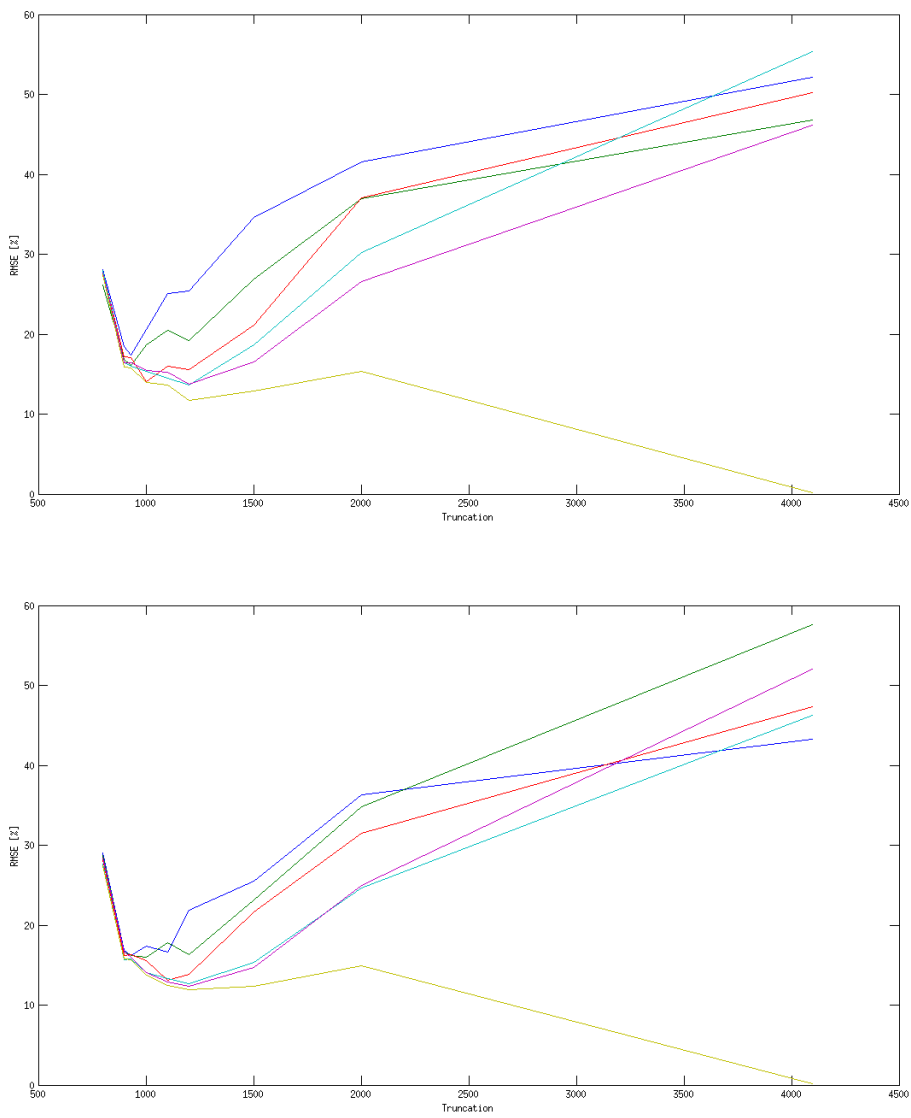Figure 7: Noiseless projections (a) and noisy projections (b) of the cylinder with $P = 16$.

Figure 8: RMSE with different truncations with normal and noisy projections. Top: $P = 16$. Bottom: $P = 32$.
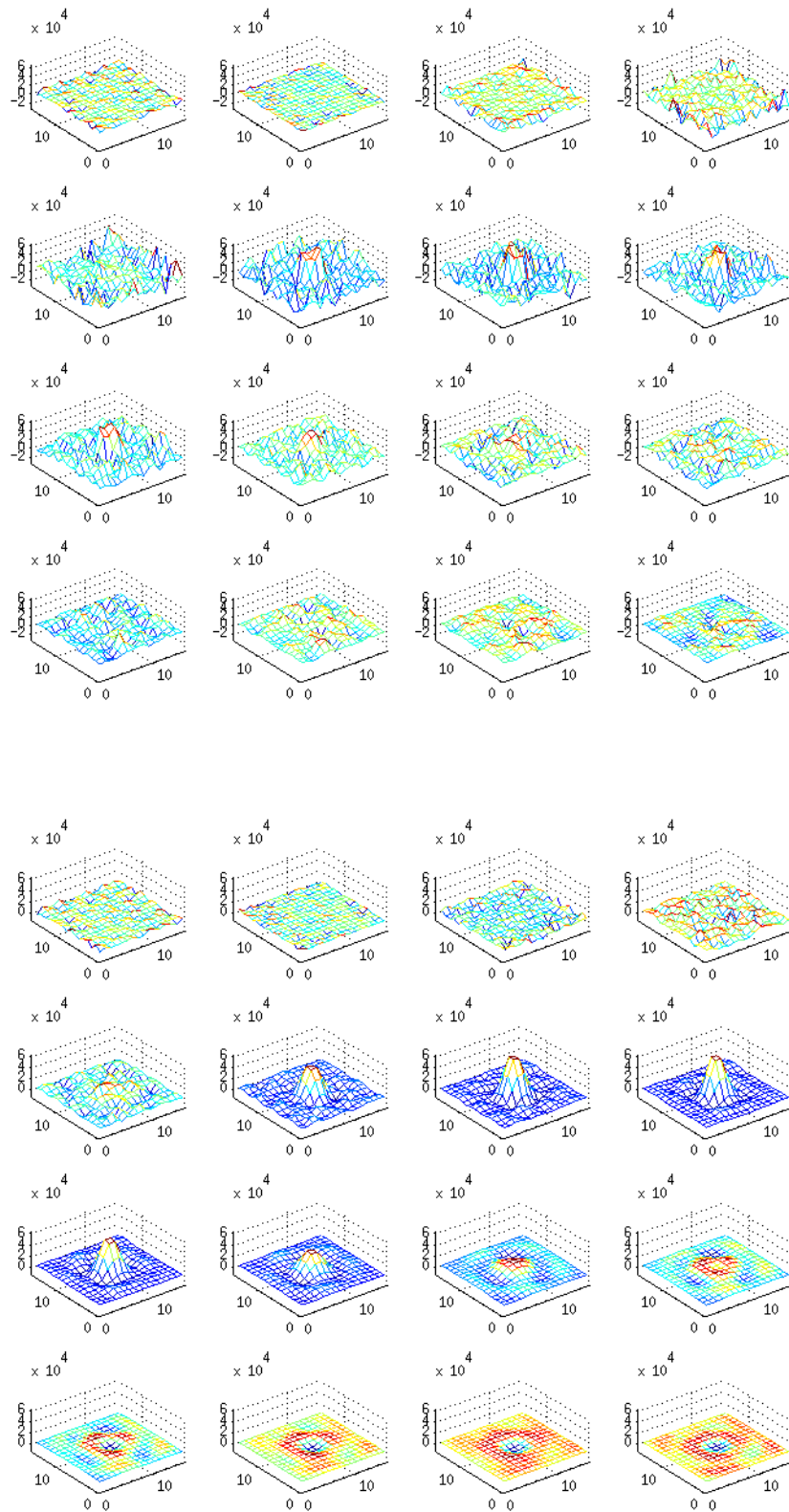
Figure 9: Reconstructions from $SNR = 9.2dB$ projections at two different truncation levels 2000 and 1200.

are also smaller for $P = 32$ in the mean over all truncation parameters (see the bottom line on Table 1). So, more available data lead to more precise solutions in the presence of noise.

6   CONCLUSIONS AND FUTURE WORK

We have presented a numerical implementation of the conical Radon transform $T\mathbb{C}$. We worked using an algebraic formulation of the direct problem to solve the inverse problem by SVD. Satisfactory reconstruction results validate our algorithm for the simulation of the direct problem. We also performed tests for data perturbed by noise using different numbers of available projections, and using TSVD as a regularization technique. We conclude that the bigger the number of projections the better are the reconstructions, but more trials should be performed to obtain more conclusive results. As a future work, we will study the pertinence of the L-curve Hansen (2000) as a decision criterion for the choice of the truncation parameter for the TSVD.

REFERENCES

Andersen A.H. and Kak A.C. Simultaneous algebraic reconstruction technique (sart): a superior implementation of the art algorithm. *Ultrasonic Imaging*, (6):81–94, 1984.

Burden R. and Faires D. Brooks/Cole CENGAGE Learning, Boston, MA, USA, 2010.

Cebeiro J. and Morvidone M. *The 2D Compounded Conical Radon Transform and its Algebraic Inversion*. Actas de la XV Reunião de Trabajo en Procesamiento de la Informaçõn y Control, Bariloche, 2013a.

Cebeiro J. and Morvidone M. Svd inversion for the bi-dimensional conical radon transform. *Journal of Physics: Conference Series*, 447, 2013b.

Cebeiro J., Morvidone M., and Rubio D. *Proc. 4th Congress on Industrial Computational and Applied Mathematics*. ASAMACI, Buenos Aires, 2013.

Delarbre J.L. *Imagerie d'émission gamma: Nouvelles méthodes d'exploitation du rayonnement diffusé*. Ph.D. thesis, Université de Cergy-Pontoise, 2005.

Driol C. *Imagerie par rayonnement Gamma diffusé à haute sensibilité*. Ph.D. thesis, Université de Cergy-Pontoise, 2008.

Guan H. and Gordon R. A projection access order for speedy convergence of art (algebraic reconstruction technique): a multilevel scheme for computed tomography. *Phys. Med. Biol.*, (39):2005–22, 1994.

Hansen C. *The truncated SVD as a method for regularization*. Stanford University, Stanford University Stanford, CA, USA, 1986.

Hansen P.C. The l-curve and its use in the numerical treatment of inverse problems. In *in Computational Inverse Problems in Electrocardiology, ed. P. Johnston, Advances in Computational Bioengineering*, pages 119–142. WIT Press, 2000.

Herman G. and Mayer L. Algebraic reconstruction techniques can be made computationally efficient. *IEEE Trans. on Med. Imaging*, 12(3):600–9, 1993.

Lu W. and Yin F.F. Adaptive algebraic reconstruction technique. *Medical Physics*, 12(31):3222–30, 2004.

Morvidone M., Nguyen M.K., Truong T.T., and Zaidi H. On the v-line radon transform and its imaging applications. *International Journal of Biomedical Imaging, doi:10.1155/2010/208179*, page doi:10.1155/2010/208179, 2010a.

Morvidone M., Nguyen M.K., Truong T.T., and Zaidi H. *Proc. 17th IEEE Int. Conf. on Image Processing*, pages 629–32. IEEE, Hong Kong, 2010b.

Morvidone M., Nguyen M.K., Truong T.T., and Zaidi H. Scattered radiation emission

imaging: principles and applications. *International Journal of Biomedical Imaging, doi:10.1155/2011/913893*, page doi:10.1155/2011/913893, 2011.

Nguyen M.K. and Truong T.T. On an integral transform and its inverse in nuclear imaging. *Inverse Problems*, 18(1):265–77, 2002.

Nguyen M.K. and Truong T.T. *Imagerie par Rayonnement Gamma Diffusé*. Hermes Science Publishing, France, 2006.

Nguyen M.K., Truong T.T., Bui H.D., and Delarbre J.L. A novel inverse problem in Îş-rays emission imaging. *Inverse Problems in Science and Engineering*, 12(2):225–246, 2004.

Nguyen M.K., Truong T.T., and Grangeat P. Radon transforms on a class of cones with fixed axis direction. *J. Phys. A: Math. Gen.*, 38:8003–8015, 2005.

Selivanov V. and Lecomte R. Fast pet image reconstruction based on svd decomposition of the system matrix. *IEEE, Trans. Nucl. Sci.*, 48(3):761–7, 2001.

Shim Y.S. and Cho Z.H. Svd pseudoinversion image reconstruction. *IEEE Transactions on Acoustics, Speech and Signal Processing*, 29(4):904–9, 1981.